

https://dspace.org/

Relationship between sintering pressure and leach rate of polycrystalline diamond compacts PDGCs using central composite design CCD modelling

Sehliselo Ndlovu; Lesley Cornish; H.S.L Sithebe

https://hdl.handle.net/10539/41944
WOS

Downloaded from a DSpace repository. https://dspace.org/

International Journal of Refractory Metals and Hard Materials 124 (2024) 106854



Contents lists available at ScienceDirect

International Journal of Refractory Metals and Hard Materials

journal homepage: www.elsevier.com/locate/IJRMHM





Relationship between sintering pressure and leach rate of polycrystalline diamond compacts (PDCs) using central composite design (CCD) modelling

A. Ndlovu [a,b,*], L.A. Cornish [b], H.S.L. Sithebe [a]

[a] Element Six (Pty) Ltd, Springs 1559, South Africa
[b] School of Chemical and Metallurgical Engineering, University of the Witwatersrand, Johannesburg, South Africa, and DSI-NRF Centre of Excellence in Strong Materials, hosted by the University of the Witwatersrand, Johannesburg, South Africa

ARTICLE INFO

Keywords:
Sintering pressure
Leach rate
Polycrystalline diamond

ABSTRACT

The effect of sintering pressure on the microstructure, wear resistance and leachability of polycrystalline diamond (PDC) was studied using central composite design (CCD) modelling. Pressure and leachability had an inverse relationship due to reduced cobalt pool size and increased diamond contiguity with higher pressures. X-ray diffraction and X-ray fluorescence confirmed the selective removal of cobalt during leaching. The relationship between pressure and leachability was modelled as linear: $Y = -1.047\times + 11.139$, valid within the 5–7 GPa pressure range. For a fixed temperature of 1600 °C, the optimum leach rate was 6.1 μm/h at 5 GPa. This study provided insights into optimizing PDC design and leaching processes for improved performance.

1. Introduction

Polycrystalline diamond compacts (PDCs) are widely used cutting tools due to their exceptional hardness and wear resistance [1–3]. The manufacturing process, which involves sintering diamond powder with a cobalt binder under high pressure and high temperature (HPHT), plays a critical role in defining the final properties of the PDC [4]. The effect of sintering pressure on the microstructure and mechanical properties of PDCs has been extensively studied [5–12]. However, the influence of pressure on the leachability of the cobalt binder, a critical aspect of PDC performance, remains largely unexplored.

Leaching, a well-established industrial practice [13], involves removing a portion of the cobalt binder using strong acids such as hydrochloric acid [13–15]. This process offers significant benefits for PDC performance, particularly in enhancing thermal stability. Studies [16–21] have shown that leaching improves thermal stability by creating a diamond-only layer that facilitates efficient heat dissipation, thereby preventing premature failure due to cobalt induced graphitization or cracking. Understanding the relationship between sintering pressure and leachability is therefore essential for optimizing the design and performance of thermally stable PDCs.

This study aims to investigate the effect of varying sintering pressure on the leachability of PDCs. We will establish a quantitative link between sintering pressure and leachability using central composite design (CCD) modelling. Accurate pressure calibration is fundamental to this study, as it ensures the reliability and robustness of the CCD model. By employing calibrated pressure application, we aim to develop an informative quantitative model that accurately reflects the impact of sintering pressure on PDC leachability. This model will not only enhance our understanding of the interaction between pressure and leachability but also guide the development of optimized leaching processes for improved PDC performance.

2. Experimental procedure

2.1. Pressure calibration

To calibrate a 6 × 32,000KN hinge-type cubic press for diamond sintering, reference diamond samples of sufficient size to be measured with a micrometre were sintered at 1500 °C under controlled loads. The resulting change in sample volume relative to the initial volume, ($\Delta V/V_0$), was accurately measured using the micrometre. Three distinct calibration points were established, linking specific pressure values to corresponding observed volume changes ($\Delta V/V_0$): 0.980 (4 GPa), 0.903 (6 GPa), 0.813 (8 GPa). The established calibration points effectively covered the typical 5–7 GPa pressure range required for diamond sintering, ensuring the calibration's practical relevance.

These calibration points formed the basis of a pressure-volume

* Corresponding author at: Element Six (Pty) Ltd, Springs 1559, South Africa.
E-mail address: fgm.ndlovu@gmail.com (A. Ndlovu).

https://doi.org/10.1016/j.ijrmhm.2024.106854
Received 9 May 2024; Received in revised form 9 July 2024; Accepted 19 August 2024
Available online 22 August 2024
0263-4368/© 2024 The Author(s). Published by Elsevier Ltd. This is an open access article under the CC BY-NC-ND license (http://creativecommons.org/licenses/by-nc-nd/4.0/).

shrinkage relationship (P—V relationship). A linear extrapolation of this relationship was employed to create a calibration curve, allowing for the estimation of sample pressure based on measured relative volume changes during subsequent sintering experiments.

2.2. Temperature monitoring

Temperature monitoring during PDC sintering was achieved using an S-type thermocouple, calibrated with a Memocal 2000, and a data logger for readout. Due to the lack of built-in cold junction compensation in the data logger, a reference junction temperature was used to compensate for this effect. The thermocouple was inserted into a hole drilled in the pyrophyllite block, positioned 0.5 mm from the sample to avoid direct contact and potential heat transfer or damage. The hole diameter was intentionally larger than the thermocouple sheath to facilitate placement and minimize heat conduction along the cable. A high-temperature ceramic tube filled the gap around the thermocouple to enhance thermal contact. Power input (kW) was used to control heat generation, and temperature monitoring provided feedback to ensure the desired sintering temperature was achieved. This feedback loop allowed for adjustments to the power input as needed to maintain the temperature within the setpoints.

2.3. Sintering of PDC

Diamond powder (10 μm average particle size) and cemented carbide substrates (WC-13%Co, 6 μm average particle size) were used as starting materials. The diamond powder was placed onto the substrate and sintered at 5 GPa, 6 GPa, and 7 GPa at a fixed temperature of 1600 °C for 15 min using a 6 × 32,000KN hinge-type cubic press cubic press (Fig. 1).

After sintering, the samples were processed to 16 mm diameter, 13 mm height and 3 mm diamond thickness, with the latter achieved by lapping. A CNC OD grinding machine was used to remove the metal cans and reduce the outer diameter from 18 mm to 16 mm. A CNC height-grinding machine was used to reduce the base of the WC substrate from 15 mm to 13 mm.

Microstructures of the PDC samples were examined using a Zeiss Evo15 scanning electron microscope at an accelerating voltage of 10 keV. Image analysis (ImageJ software) was used to measure the aspect ratio (AR) and Feret diameter (FD) of the cobalt pools (all the Co regions). The AR gave an indication of cobalt pool shape while the FD gave an indication of cobalt pool size. The AR is defined as the ratio of the length to the width of the particle and was derived from the ratio of the major and minor axis of a fitted ellipse. The FD is defined as the distance between two parallel tangents of the particle at different arbitrary angles and was derived from the longest distance between any two parallel points of the particle. The cobalt content and contiguity were calculated from the SEM-BSE micrographs using ImageJ on 16 images for each specimen at 1000× magnification and SIS-pro software. Calculations of the cobalt content and contiguity were done using MathConnex 2000 with MathCad 2000 Professional.

Wear resistance was evaluated using a vertical turning lathe (VTL) test with a 5000 N normal load and 1.8 m/s cutting speed. Wear scar areas were measured using an optical profilometer and ZEN Core software. The amount of wear can be measured in different ways, most of which involve measurement of either mass change or the size of a worn region (wear scar). However, for PDCs, wear scar dimensions are commonly reported as an area of the wear scar since PDC wear scars are large enough to measure and the area of the worn region can be clearly differentiated for materials with different wear resistances.

2.4. Leaching of PDC

The sintered and machined samples were placed in a Teflon container with 0.2 M HCl solution and heated at 110 °C for 96 h. Leach depths were measured using X-ray tomography (XRT, X-TEK XTV160, United Kingdom).

XRD was performed using PANalytical X'Pert^3 to analyse the phases of the leached and un-leached PCD samples. The Reference Intensity Ratio (RIR) method was used to calculate relative phase amounts. RIR is semi-quantitative and was suitable for assessing the relative proportions of cobalt and tungsten phases between un-leached and leached PCD samples. XRF was performed using PANalytical ZETIUM to determine the cobalt to tungsten ratio (Co/W) of the leached and un-leached PCD samples.

2.5. Central composite design (CCD) modelling

All modelling was carried out using central composite design (CCD) on Minitab 19 software. The design matrix is presented in Table 1. The α value is the calculated distance of each individual axial point from the centre in the CCD [23–25]. When α is <1, the axial point is within a cube, and if >1, the axial point is outside the cube. The two-level full factorial usually contains >2-level factors. [23–25]. Two factors were considered in the central composite design: sintering pressure (X_1), and sintering temperature (X_2).

The modelled response function was the leach rate and CCD used a quadratic Eq. [25] to approximate how changes in the process variables affected the leach rate:

$$Y = \beta_0 + \sum_{i=1}^{3} \beta_i X_i + \sum_{i=1}^{3} \beta_{ii} X_i^2 + \sum_{\substack{i=1 \\ i<j}}^{3} \beta_{ij} X_i X_j \quad (1)$$

where Y = estimated response; β_0 = constant, β_i = coefficient for the linear terms, β_{ii} = coefficient for the quadratic terms and β_{ij} = coefficient for the interactive terms. The validity of the model was confirmed using the correlation coefficient (R2), to indicate how well the model equation fitted the data. The accuracy of the model was assessed by calculating the percentage variation using Eq. 2, which estimated how close the modelled data matched the experimental data. Quantifying the accuracy

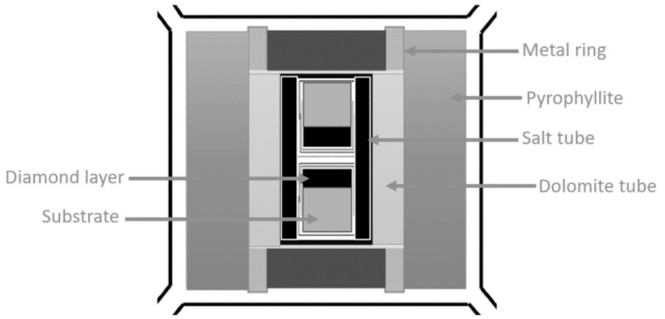


Fig. 1. *Schematic diagram of the cubic press capsule used for sintering* [22].

Table 1
Summary of the central composite design matrix.

Description	
Factors	2
Base runs	13
Base blocks	1
Replicates	1
Total runs	13
Alpha (α)	1.41421
Cubic points	4
Centre points in cube	5
Axial points	4
Centre points in axial	0

of the mathematical model was the most critical process to justify using the model.

$$\%\text{variation} = (|\text{modelled value} - \text{experimental value}|/\text{modelled value}) \times 100 \quad (2)$$

3. Results

Fig. 2 shows the X-ray map of the 6 GPa sample, with diamond surrounding cobalt pools. Some of the cobalt pools also contained tungsten. Table 2 shows the EDX analyses of diamond, cobalt and tungsten.

Fig. 3 shows the microstructures of the diamond layer of the 5 GPa, 6 GPa and 7 GPa samples, showing the cobalt pools between the diamond grains. The larger cobalt pools were elongated while the smaller ones were rounder (Fig. 3). The cobalt pools for the 8 GPa sample were the smallest, while those for the 5 GPa sample were the largest (Fig. 3).

The derived cobalt pool sizes (FD) and shape (AR) are presented in Table 3. The FD of the cobalt pools decreased with increased sintering pressure, as did the AR, as shown in Fig. 3.

Table 4 shows the cobalt content measurements from image analysis, where the cobalt content in the diamond layer decreased with increased pressure.

Table 4 also shows the relationship between contiguity, the calculated amount of diamond-to-diamond contact (diamond neck), and sintering pressure. Better diamond contiguity was achieved after sintering at elevated pressure.

Table 5 shows the wear scar measurements of the samples: the 5 GPa sample had the largest wear scar and the 7 GPa sample had the smallest wear scar. The 6 GPa sample had the lowest standard deviation.

Fig. 4 shows the ANOVA analysis for the measurements of the wear scars. The 5 GPa sample overlapped with the 6 GPa sample, and the 6 GPa sample overlapped with the 7 GPa sample. However, the 5 GPa and 7 GPa samples did not overlap, which was supported by their *p*-value (probability) of 0.003, which was less than the standard significance value of 0.05, indicating that the bell-curves did not overlap.

Table 6 shows the leach depths measurements after 96 h leaching, where the 5 GPa sample had the highest leach depth and the 7 GPa sample had the lowest leached depth. The 7 GPa sample had lowest standard deviation.

Fig. 5 shows the ANOVA analysis for the average values of the leach depths, showing that the bell-curve for the 7 GPa sample was closer to the 8 GPa sample than the 5 GPa samples, and none overlapped, although the 6 and 7 GPa samples were close. The ANOVA analysis had a *p*-value of 0.001 for the 5 GPa and 7 GPa samples, indicating that the bell-curves did not overlap.

Fig. 6 shows the relationship between the leach rate and pressure for determining the mathematical model to predict the leachability as function of pressure. The 6 GPa sample had the lowest standard deviation.

Fig. 7 shows that both the leached and un-leached PCD samples contain the cobalt phase (Co3W), tungsten phase (WC) and diamond (C).

Table 7 shows the RIR quantitative phase analysis indicating the relative amount of cobalt and tungsten phases between un-leached and leached PCD samples.

Table 8 shows the XRF analysis, indicating the cobalt to tungsten (Co/W) ratio for the leached and un-leached samples.

4. Discussion

4.1. Effect of pressure on as-sintered microstructures

Increased pressure during sintering reduced both average cobalt pool size (Fig. 3, Table 3) and contiguous region size (Fig. 4). This phenomenon can be attributed to enhanced plastic deformation and rearrangement of diamond particles at higher pressures. These processes occur during the cold and hot compaction stages, leading to pore shrinkage and decreased FD of the cobalt pools [10]. Furthermore, smaller pores

Table 2
EDX results of samples pressed at 5 GPa, 6 GPa and 7 GPa.

Sample	Diamond (wt%)	Cobalt (wt%)	Tungsten (wt%)
5 GPa	84.0 ± 1.1	13.7 ± 2.3	2.3 ± 1.1
6 GPa	86.8 ± 1.1	10.5 ± 1.9	2.7 ± 1.4
7 GPa	89.1 ± 0.9	8.8 ± 2.0	2.1 ± 1.2

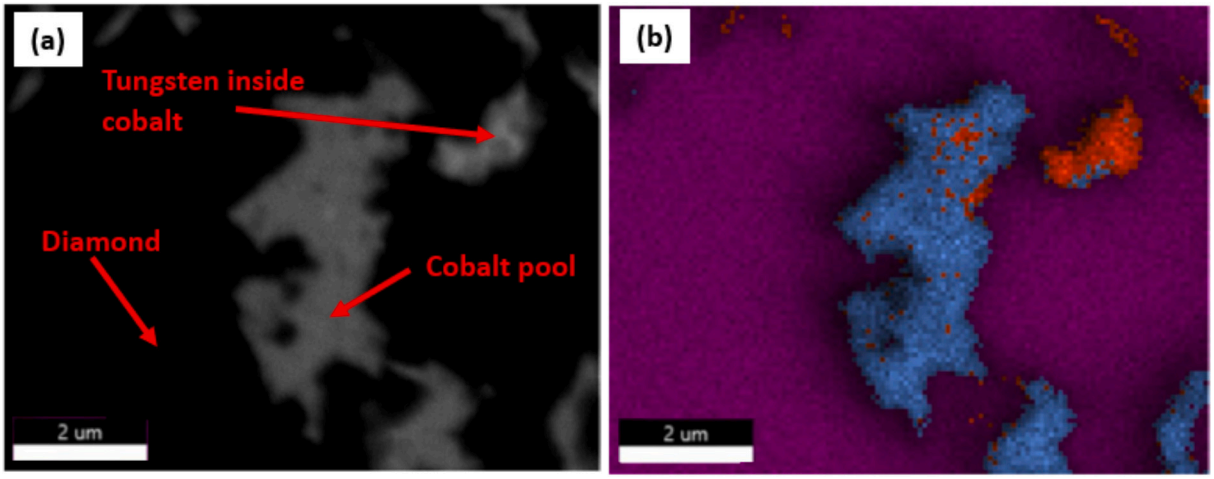


Fig. 2. 6 GPa sample: (a) SEM-BSE image showing diamond (dark), cobalt (medium grey) and tungsten (light) and (b) X-ray map showing cobalt (blue), tungsten (orange) and diamond (purple). (For interpretation of the references to colour in this figure legend, the reader is referred to the web version of this article.)

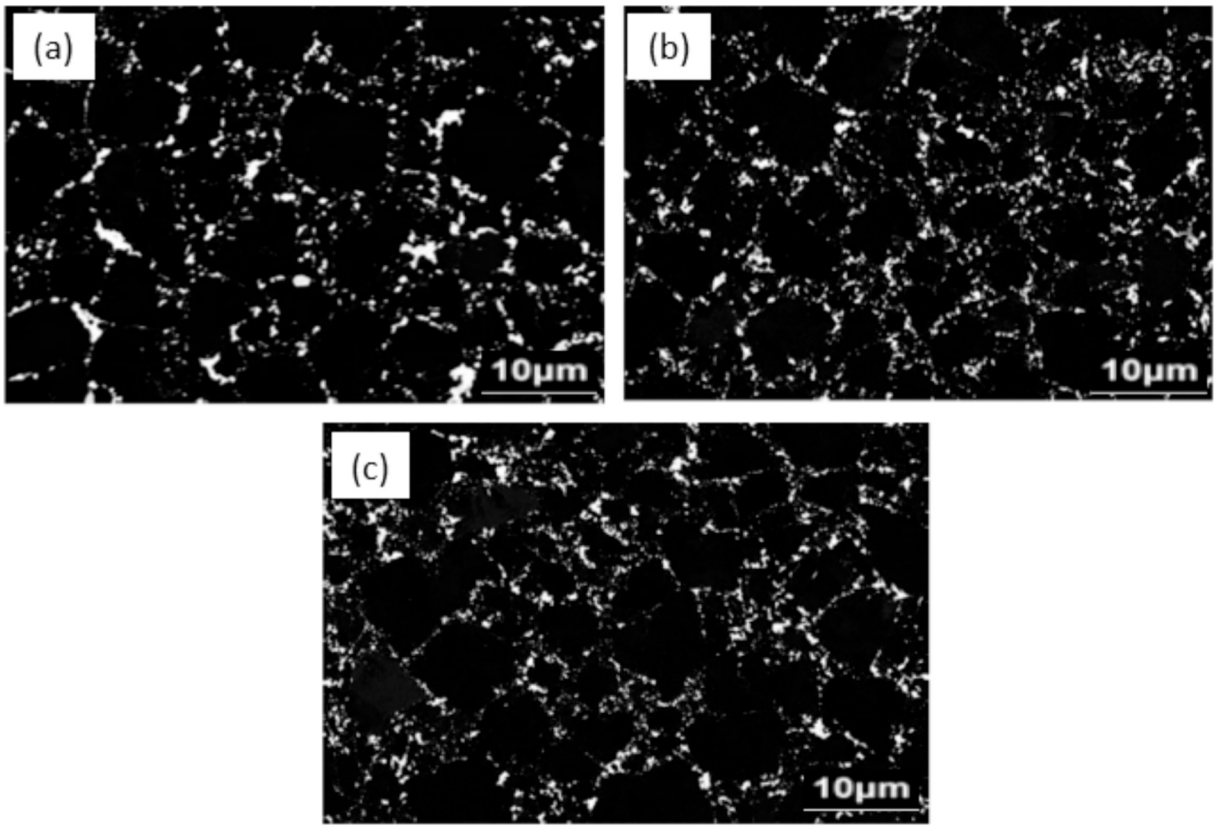


Fig. 3. SEM-BSE images of PDC binder pools at the top of the layer at different pressures: (a) 5 GPa, (b) 6 GPa and (c) 7 GPa, showing cobalt pools (light contrast) and diamond (dark contrast).

Table 3
Average cobalt pool size and shape at different pressures.

Sample	Cobalt pool aspect ratio	Cobalt Pool Feret Diameter (μm)
5 GPa	9.1 ± 2.2	2.36 ± 0.16
6 GPa	7.6 ± 2.1	1.64 ± 0.13
7 GPa	4.9 ± 2.7	1.06 ± 0.09

Table 4
Quantitative image analysis of the 5 GPa, 6 GPa and 7 GPa samples.

Sample	Cobalt (Vol%)	Contiguity (%)
5 GPa	9.2 ± 0.9	61.4 ± 1.8
6 GPa	7.8 ± 0.7	64.3 ± 0.9
7 GPa	6.1 ± 0.8	66.9 ± 1.7

limited cobalt infiltration into the diamond layer, resulting in smaller binder pools (Table 3). This trend is shown by the 7 GPa sample which had the smallest pores before infiltration (Fig. 3), allowing for minimal cobalt infiltration and consequently, the smallest average cobalt pool size (Table 3). This observation aligns with the source of cobalt, originating from the cemented carbide substrate, with the amount reaching the diamond layer being pressure- dependent.

Higher pressure also contributed to a reduction in the contiguous region (Fig. 4) due to the formation of smaller pores at the interface, resulting in fewer open structures within the contiguous region [26]. The availability of open porosity directly affects the extent of cobalt diffusion into the diamond layer. The absence of smaller diamond grains at the interface (Fig. 4) provided space for cobalt infiltration and subsequent dissolution of diamond grains, creating an open structure [26]. This agrees with the 7 GPa sample having the least pre-infiltration porosity, limiting the amount of cobalt that could infiltrate the diamond layer, thus leading to the formation of the smallest cobalt pools. The relationships between pressure, pore size and cobalt infiltration is further supported by Fig. 4 and Table 3, where smaller pore sizes associated with higher pressure had limited cobalt infiltration.

The 5 GPa sample exhibited the highest cobalt content at 9.2 ± 0.9 vol% (Table 4), agreeing with Westraadt et al. [27], who had a similar cobalt content (9.0 ± 1.0 vol%) for a PDC sintered at 5.5 GPa. While Westraadt et al. [27] did not report diamond contiguity for their sample, it is reasonable to expect similar values to the 5 GPa sample in Table 4, given the comparable cobalt content. Additionally, the present findings are consistent with Dai et al. [28], who observed a cobalt content of 10.7 ± 0.1 vol% for a sample sintered at 5.5 GPa. Thus, high pressure reduced pre-infiltration porosity, limiting the amount of cobalt that could infiltrate the diamond layer resulting in reduced cobalt content.

This investigation agreed with previous findings [26,27,30] that cobalt content significantly reduced the wear resistance of polycrystalline diamond composites (PDC). As expected, the sample exhibiting the highest cobalt content (5 GPa) had the lowest contiguity (Table 4) and the poorest wear resistance. This agrees with industrial experience [26,28,29], which shows that both high cobalt content and reduced contiguity are associated with reduced wear resistance. This can be attributed to the role of cobalt as a binder during PDC sintering. Cobalt facilitates the overall sintering process, which involves the dissolution of graphite from the diamond grain surfaces followed by its

Table 5
VTL measurements of the area of the wear scars on the sintered samples.

Pressure	Wear scar area (mm^2)	Minimum	Maximum
5 GPa	12.7 ± 1.5	11.0	14.1
6 GPa	7.4 ± 0.8	6.6	8.2
7 GPa	3.1 ± 1.0	1.9	4.0

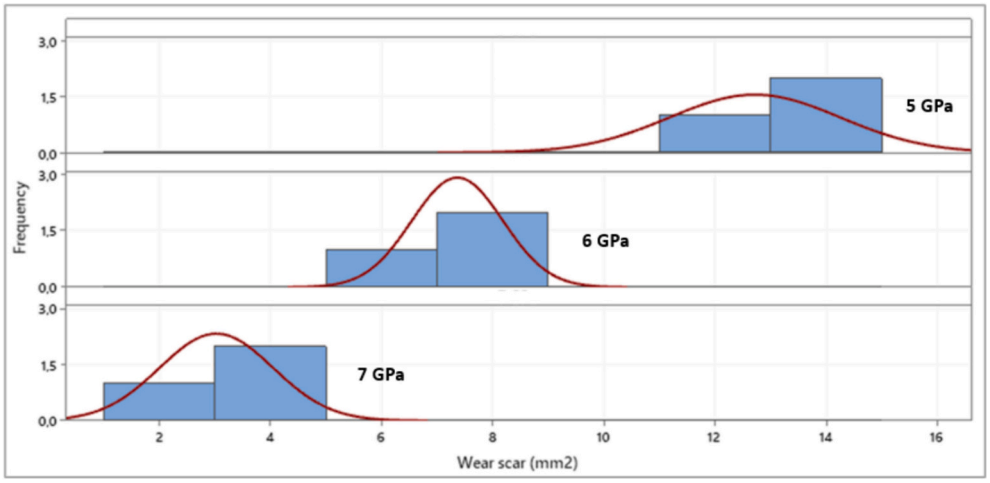


Fig. 4. ANOVA analysis of the wear scar measurements at different pressures.

Table 6
Average leach depth measurements (μm) for 20 measurements.

Pressure	Leach depth (μm)	Minimum	Maximum
5 GPa	744.1 ± 37.8	671.0	811.0
6 GPa	459.4 ± 26.3	420.0	538.0
7 GPa	328.7 ± 13.4	303.0	349.0

reprecipitation as diamond, ultimately forming diamond-to-diamond bonds and diamond intergrowth between the grains (Fig. 3) [4]. This process results in the formation of necks, or new diamond grain connections, between the original diamond grains [4].

4.2. Effect of pressure on wear resistance

The relationship between sintering pressure and wear scar area is presented in Table 5. The wear scar area of the PDC samples decreased significantly from 12.7 mm^2 to 3.1 mm^2 as the sintering pressure increased from 5 GPa to 7 GPa (Table 5). The one-way analysis of variance (ANOVA) of the average wear scar sizes gave a statistically significant difference between the 5 GPa, 6 GPa and 7 GPa (Fig. 4), shown by the *p*-value (0.003) being lower than the chosen significance level ($\alpha = 0.05$) and the clear separation of standard deviations in Fig. 4. This inverse correlation is attributed to increased diamond-diamond contact points (Table 4) and reduced cobalt pool size (Table 3), resulting in a more wear-resistant structure. However, this increased wear resistance comes at the cost of slower leaching rates (Table 6), as the denser, less porous material hinders acid access to the binder during leaching [13]. Therefore, a trade-off exists between wear resistance and leaching efficiency in PDC manufacturing.

4.3. Leached PCD layer versus un-leached PCD layer

Table 7 showed the RIR values of the changes in the relative amount of the cobalt phase (Co_3W) and tungsten phase (WC) between the un-leached and leached PCD layer samples. The RIR of cobalt phase decreased significantly from 0.9 in the un-leached sample to 0.2 in the leached sample (Table 7). This indicated a substantial reduction of approximately 78% in the relative amount of cobalt phase after the

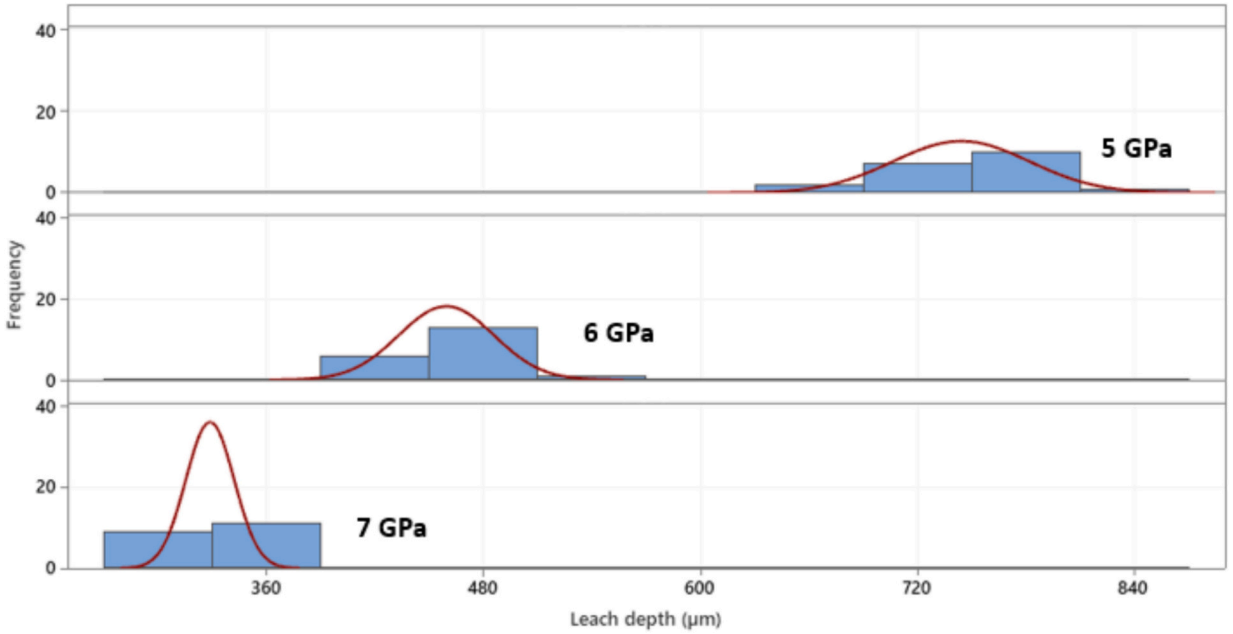


Fig. 5. ANOVA analysis of the leach depth measurements.

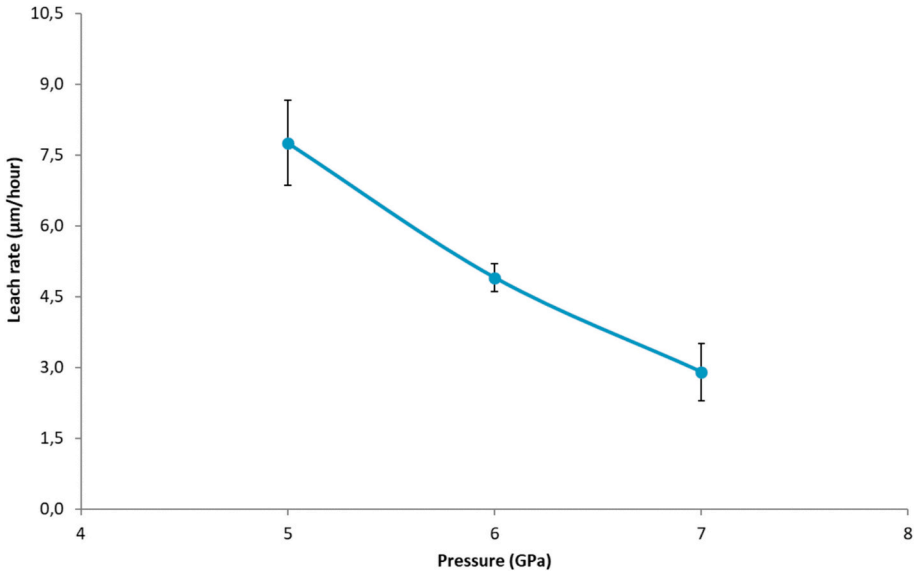


Fig. 6. Relationship between leachability (leach rate) and sintering pressure after 96 h of leaching in HCl acid.

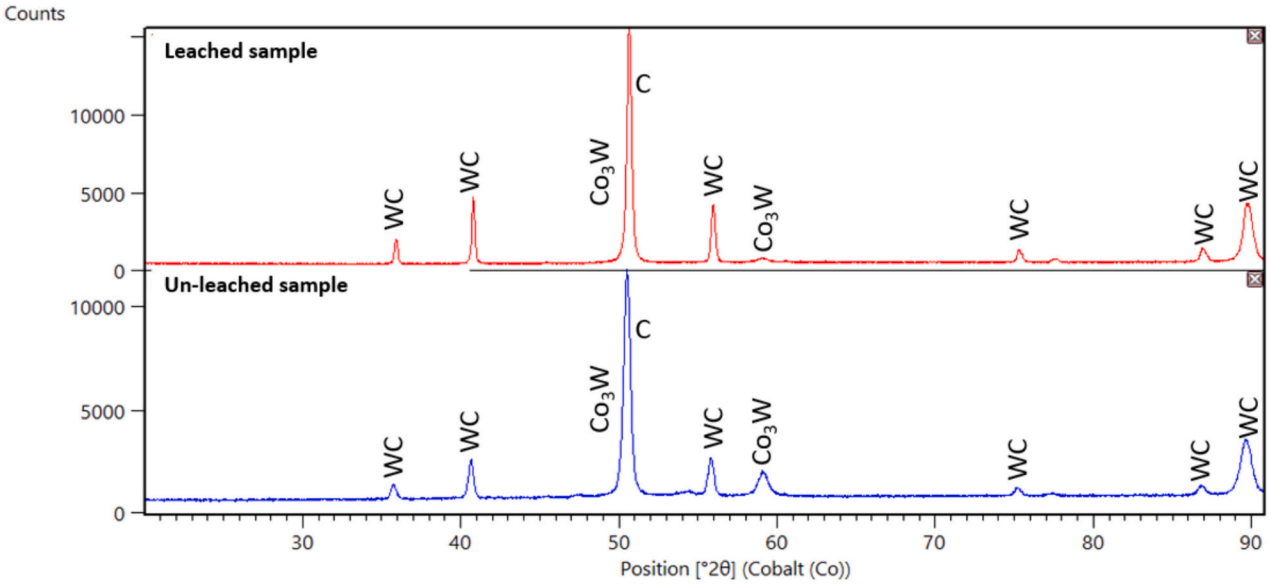


Fig. 7. XRD patterns for the leached and un-leached PCD layer samples.

Table 7
Reference Intensity Ratio (RIR) values for the leached and un-leached PCD layer samples.

RIR	Leached PCD	Un-leached PCD
Cobalt phase (Co_3W)	0.20 ± 0.01	0.91 ± 0.03
Tungsten phase (WC)	1.11 ± 0.02	1.21 ± 0.01

leaching process. This suggested that the leaching process effectively removed a large portion of the cobalt phase. The RIR of the tungsten phase remained relatively constant, decreasing only slightly from 1.2 in the un-leached sample to 1.1 in the leached sample (Table 7). This indicated that the leaching process had a minimal impact on the relative amount of the tungsten phase, suggesting that it is more resistant to the leaching conditions than the cobalt phase. The leaching process appeared to be highly selective, primarily targeting and removing the cobalt phase while leaving the tungsten phase largely unaffected. This selectivity was due to differences in the chemical stability and solubility of the two phases in the HCl leaching environment. The significant reduction in the cobalt phase suggested that it is more susceptible to dissolution under these conditions, while the minimal change in WC indicates its greater resistance to leaching.

Table 7 showed a substantial reduction of approximately 78% in the relative amount of cobalt phase after the leaching process. However, the remaining 22% suggested that a fraction of the cobalt phase was not accessible to the HCl acid during the leaching process. This inaccessible cobalt phase is located within closed pores or cavities within the PCD

Table 8
XRF results showing the cobalt to tungsten ratio (Co/W) between leached and un-leached samples.

Parameter	Leached PCD	Un-leached PCD
Co/W Ratio	0.23 ± 0.01	0.46 ± 0.03

material [8]. These closed pores can act as protective barriers, preventing the acid from reaching and dissolving cobalt encapsulated within them. The presence of closed porosity in PCD is due to coalescence: During sintering, smaller pores can coalesce to form larger pores, some of which may become isolated from the surface and remain closed [8].

Table 8 showed a significant change in the cobalt to tungsten (Co/W) ratio following the leaching process. The un-leached PCD sample exhibited a Co/W ratio of 0.46, indicating that cobalt comprised 31.6% of the total Co and W content (Table 8). After leaching, this ratio decreased to 0.23, corresponding to a cobalt proportion of 18.6%. This reduction signified a 50% decrease in the relative amount of cobalt in the PCD sample, corroborating the XRD findings and highlighting the effectiveness of the leaching process in removing a substantial portion of the cobalt-containing phase. Both techniques indicated a significant reduction in the amount of cobalt present in the PCD layer after leaching. The minor change in the RIR of WC in the XRD results was also consistent with the XRF data, which showed that the overall tungsten content remained relatively unchanged after leaching. Together, these results suggested that the leaching process primarily removed the Co_3W phase, while leaving the WC phase mostly intact. The combined XRF (Table 8) and XRD (Table 7) results provided strong evidence for the removal of cobalt from the PCD during leaching. The reduction in the Co/W ratio and the decrease in the RIR of Co_3W both indicated a significant decrease in the amount of cobalt present in the leached material.

4.4. Effect of pressure on leachability

The leachability of cobalt exhibited negative correlation with pressure (Table 6), due to the influence of cobalt pool size on acid flow pathways. Larger cobalt pools provided wider channels for acid ingress, facilitating cobalt removal. Conversely, smaller pools restricted acid flow, hindering leachability [13]. Among the investigated pressures, 5 GPa had the fastest leachability (Table 6), coinciding with the largest observed cobalt pool size (Fig. 3 and Table 4), highest cobalt content (Fig. 3 and Table 4) and lowest contiguity (Table 4). These findings show that the leachability of the cobalt binder is directly governed by the distribution and accessibility of cobalt within the pools between diamond particles [13]. Physical exposure of the binder to the leaching solution is crucial for the reaction to proceed and the extent of this exposure dictates the leaching rate.

The pores allow acid access, and smaller pores allow smaller acid volumes to pass through them in a given time, and hence reduce leachability (Table 3). Conversely, diamond grains encapsulate some pools, effectively shielding them from the acid solution and making them unreachable. The initial leaching reaction involves chloride anions from the HCl acid interacting with surface-exposed cobalt pools on the PDC. Subsequently, these anions diffuse deeper through the intergranular pores, reacting with additional cobalt to form cobalt chloride, which remains dissolved and is ultimately removed from the system [13,31]. As cobalt is leached from these pools, they transform into pores themselves. Consequently, leachability is further influenced by the diffusion rate of anions and reaction products through these newly formed inter-granular pores. Therefore, the size of the cobalt pools dictates both the rate-limiting step of leaching and the subsequent pore size, which in turn governs acid diffusion and access to the remaining cobalt [13,31]. Smaller pools restrict diffusion and consequently decrease the leaching rate, while larger pools facilitate diffusion and leach rate [13,31].

Leach depth measurements for the 5 GPa and 7 GPa samples exhibited normal distributions (Fig. 5). However, the normality test for the 6 GPa data set was rejected (p-value <0.05), with only one outlier identified (Fig. 5), which skewed the distribution, rendering the 6 GPa data set non-normal. One-way ANOVA identified a statistically significant difference (p-value = 0.001) in the mean leach depths among the pressure groups (Fig. 5), indicating that leach depth decreased with increasing pressure.

Table 9
Mathematical models for the relationship between pressure and leachability.

Mathematical model	K, slope	Fitted equation	Correlation coefficient (R^2)
Exponential	17.167	$Y = 17.167e^{-0.212x}$	0.9697
Linear	−1.047	$Y = -1.047\times + 11.139$	0.9847
Logarithmic	−6.221	$Y = -6221\ln(X) + 15.988$	0.9762
Polynomial	0.302	$Y = 0.302 \times {}^{2}–4.667\times + 21.813$	0.9803
Power	45.745	$Y = 45{,}745\times^{-1.263}$	0.9767

Fig. 6 shows the relationship between the leach rate and pressure. Different models were evaluated using Minitab software by fitting them to Fig. 6 and then assessing their suitability to describe the relationship between leach rate and pressure using the correlation coefficient (R^2). The five mathematical models that fitted Fig. 6 well are presented in Table 9.

The linear model had the highest R^2 value, and the exponential model had the lowest R^2 value. The R^2 value indicated how well the model equation fitted the data: stronger relationships were closer to 1 and weaker relationships were closer to zero. The equation that had the closest to perfect fit for the experimental data (Fig. 6) was the linear model ($R^2 = 0.9847$), implying that 98.47% of the variability in leach rate was explained by the mathematical model. Thus, under the experimental conditions tested, the effect of pressure on the leach rate and pressure can be modelled by:

$$Y = -1.047 \times + 11.139 \quad (3)$$

where:

Y = leach rate.

X = sintering pressure.

In Table 7, the slope, K, describes the extent to which sintering pressure affected the leach rate, and the intercept is the value of the leach rate when the sintering pressure is 0 GPa. However, the value of the intercept was neglected because sintering pressure would never be 0 GPa since the typical boundary sintering conditions to sinter a commercial PDC starts from 5 GPa [9]. Also, moving the intercept to zero would have affected the accuracy of the model for prediction within the boundary sintering conditions of 5 GPa – 7 GPa.

To validate Eq. 3 (relationship between leach rate and sintering pressure), samples sintered at 6.8 GPa and 8 GPa were leached for 96 h. These two pressures were chosen because 6.8 GPa was within the sintering boundary conditions tested, whereas 8 GPa was outside. Thus, the 6.8 GPa sample validated the suitability of the model to predict leach rates within the boundary conditions, while the 8 GPa sample validated the suitability of the model to predict leach rates outside the boundary conditions. Pressures <5 GPa were not validated because most commercial products are sintered at or above 5 GPa.

A comparison of modelled and experimental data is presented in Table 10. For the 6.8 GPa sample, the modelled value deviated from the experimental value by 2.4%, indicating good agreement within the established boundary conditions (Eq. 3). Conversely, at 8 GPa, the model over-predicted the experimental value by 62%, indicating a significant limitation in predictive accuracy beyond the defined pressure range (>7 GPa). This agrees with the increased standard deviations of

Table 10
Validation of the modelled data against the experimental data after 96 h of leaching.

Pressure (GPa)	Modelled value (μm/h)	Experimental value (μm/h)	Variation (%)
6.8	4.03	4.12 ± 0.44	2.4
8	2.76	1.05 ± 0.17	61.9

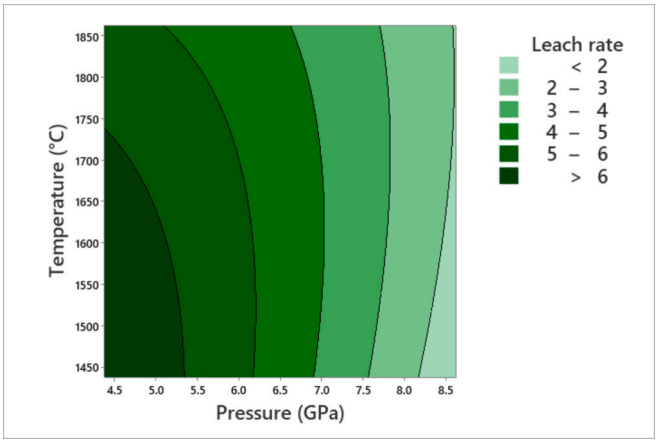


Fig. 8. Contour plot model, showing how sintering conditions affect leachability.

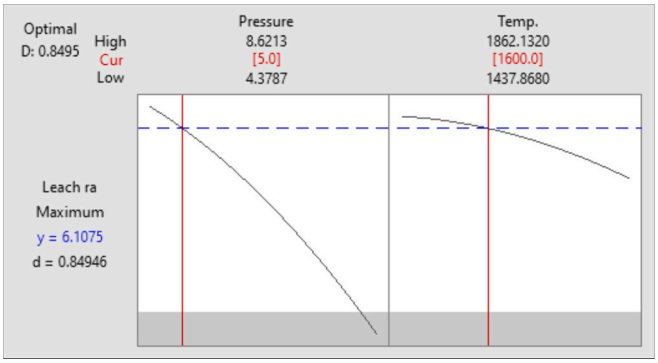


Fig. 9. Response optimization model, showing maximum leachability achievable under the experimental boundary conditions tested, where: high = maximum value of the pressure and temperature, low = lowest value of the pressure and temperature and cur = current value of the pressure and temperature.

the boundary limits in Fig. 6.

Fig. 8 shows the contour plot modelled using central composite design (CCD) with Minitab on the experimental conditions. The plot indicates that higher pressures and higher temperatures would have lower leachability, which agrees with Fig. 6.

A response optimization model was developed using Minitab to investigate the influence of pressure and temperature on leach rate (Fig. 9). The model indicated that pressure exerted a greater influence on leach rate than temperature within the investigated range of 5–7 GPa. The maximum predicted leach rate of 6.1 μm/h was achievable at 5 GPa and 1600 °C. While the model suggests that lower pressures can promote higher leachability, it is important to consider the trade-off between pressure and other factors impacting material properties. As shown in Table 4, lower pressures can also lead to the formation of larger cobalt pools and lower contiguity, which compromises wear resistance. Therefore, an optimal operating pressure needs to be established that balances the desired leach rate and the required mechanical properties.

5. Conclusions

This study investigated the effect of sintering pressure on the microstructure, wear resistance and leachability and found that increased sintering pressure reduced cobalt pool size, increased contiguity, reduced leachability and increased wear resistance. The relationship between sintering pressure and leachability was modelled using CCD modelling within the boundary conditions of 5–7 GPa, to predict PDC leachability, and then estimated the required leach rates for target leach depths. The conclusions were:

- Increased pressure enhances wear resistance but reduces leachability.
- HCl leaching selectively removes cobalt while leaving tungsten unaffected.
- The relationship between pressure and leachability was modelled as linear: $Y = -1.047\times + 11.139$, valid within the 5–7 GPa pressure range.
- At 1600 °C, the optimum leach rate was 6.1 μm/h within the boundary conditions of 5–7 GPa.

CRediT authorship contribution statement

A. Ndlovu: Writing – original draft, Software, Project administration, Methodology, Investigation, Formal analysis, Data curation. **L.A. Cornish:** Writing – review & editing, Visualization, Validation, Supervision. **H.S.L. Sithebe:** Resources, Project administration, Funding acquisition, Conceptualization.

Declaration of competing interest

The authors declare that they have no known conflict of interests in regard to the manuscript entitled " Relationship between sintering pressure and leach rate of polycrystalline diamond compacts (PDCs) using Central Composite Design (CCD) ".

Data availability

Data will be made available on request.

Acknowledgments

This work was funded by Element Six, South Africa.

References

[1] H. Huang, B. Zhao, W. Wei, Z. Si, K. Huang, Effect of cobalt content on the performance of polycrystalline diamond compacts, Int. J. Refract. Met. Hard Mater. vol. 92 (2020), https://doi.org/10.1016/j.ijrmhm.2020.105312 article no: 105312, Nov.
[2] J. Gu, K. Huang, Role of cobalt of polycrystalline diamond compact (PDC) in drilling process, Diam. Relat. Mater. 66 (2016) 98–101. Jun, https://doi.org/10.1016/j.diamond.2016.03.025.
[3] K. Francis, Effect of Carbide Additives on the Structure and Behaviour of Polycrystalline Diamond, PhD, University of Pretoria, 2017.
[4] J.E. Westraadt, I. Sigalas, J.H. Neethling, Characterisation of thermally degraded polycrystalline diamond, Int. J. Refract. Met. Hard Mater. 48 (2015) 286–292, https://doi.org/10.1016/j.ijrmhm.2014.08.008.
[5] V. Kanyanta, S. Ozbayraktar, K. Maweja, Effect of manufacturing parameters on polycrystalline diamond compact cutting tool stress-state. International journal of refractory metals and hard materials, Int. J. Refract. Met. Hard Mater. 45 (2014) 147–152.
[6] M. Akaishi, T. Ohsawa, S.Y. Amaoka, Synthesis of fine-grained polycrystalline diamond compact and its microstructure, J. Am. Ceram. Soc. 74 (1) (1991) 5–10.
[7] S. Middlemiss, Polycrystalline Diamond with Improved Abrasion Resistance, Patent, US0140132A1, 2004.
[8] R.M. German, Liquid Phase Sintering, Springer Science & Business Media, Berlin, Germany, 2013.
[9] J.M. Fuller, PDC cutter with stress diffusing structures, Patent WO2009024752A2 (2009).
[10] E.G. Minnaar, Characterisation of Ultra-High Pressure Polycrystalline Diamond, PhD, Nelson Mandela University, 2019.
[11] Liu S., Han N., Zou Y., Zhu P., and Liu B., "Polycrystalline diamond compact with enhanced thermal stability," J. Mater. Sci. Technol., vol. 33, no. 11, pp. 1386–1391, Nov. 2017, doi: https://doi.org/10.1016/j.jmst.2017.03.014.
[12] Y. Zhang, High pressure and high temperature sintering of fine-grained PCD using bi-layered assembly, High Pressure Res. 29 (2009) 235–334.
[13] K. Davis, R. Frazier, J. Fischer, Sonochemical leaching of polycrystalline diamond, Patent, US0169419 A1, 2007.
[14] K. Naidoo, G.J. Davies, J.L. Myburgh, Method of making polycrystalline diamond material, Patent, US20130291443 A1, 2013.

[15] K. Naidoo, J.H. Liversage, D.E. Scott, H.S.L. Sithebe, B.A. Kaiser, M.L. Fish, Polycrystalline diamond element, Patent, US0061149A1, 2012.
[16] C.S. Montross, K. Naidoo, Polycrystalline Diamond Material, Patent, US0326963A1, 2013.
[17] K. Naidoo, Polycrystalline diamond material, Patent, US0333300A1, 2013.
[18] B. Bhushan, Principles and Applications of Tribology, John Wiley and Sons, New York, USA, 1999.
[19] S. Masethe, PDC Wear Testing, Report, Springs, South Africa, 2014.
[20] Randall G.M., Suri P., and Park S. J., "Review: liquid phase sintering," J. Mater. Sci., vol. 44, no. 1, pp. 1–39, Jan. 2009, doi: https://doi.org/10.1007/s10853-008-3008-0.
[21] G. Udupa, S.S. Rao, K.V. Gangadharan, Functionally graded composite materials: an overview, Procedia Mater. Sci. 5 (2014) 1291–1299, https://doi.org/10.1016/j.mspro.2014.07.442.
[22] V. Kanyanta, A. Dormer, N. Murphy, A. Invankovic, Impact fatigue fracture of polycrystalline diamond compact (PDC) cutters and the effect of microstructure, Int. J. Refract. Met. Hard Mater. 46 (2014) 145–151, https://doi.org/10.1016/j.ijrmhm.2014.06.003.
[23] S. Ibrahim, I. Daut, Y.M. Irwan, M. Irwanto, N. Gomesh, Z. Farhana, Linear regression model in estimating solar radiation, in: Energy Procedia, Elsevier BV, 2012, pp. 1402–1412, https://doi.org/10.1016/j.egypro.2012.05.156.
[24] X.Q. Liu, Improved estimator in a linear regression model, J Stat Plan Inference 141 (1) (2011) 189–196. Jan, https://doi.org/10.1016/j.jspi.2010.05.030.
[25] S.A. Hadi, Regression Analysis by Example, Fourth edition, John Wiley and Sons, Canada, 2006.
[26] Scott T.A, "The influence of microstructure on the mechanical properties of polycrystalline diamond: a literature review," Adv. Appl. Ceram., vol. 117, no. 3, pp. 161–176, Apr. 2018, doi: https://doi.org/10.1080/17436753.2017.1389462.
[27] J.E. Westraadt, Thermal Degradation of Diamond Compacts: A TEM Investigation, PhD, Nelson Mandela University, 2011.
[28] W. Dai, S. Zhang, J. Tu, X. Wang, C. Zhao, B. Liu, Grain size dependence of wear resistance of polycrystalline diamond compact, Ceram. Int. 49 (23) (2023) 37396–37406. Dec, https://doi.org/10.1016/j.ceramint.2023.09.064.
[29] Q.S. Bai, Y.X. Yao, P. Bex, G. Zhang, Study on wear mechanisms and grain effects of PCD tool in machining laminated flooring, Int. J. Refract. Met. Hard Mater. 22 (2–3) (2004) 111–115, https://doi.org/10.1016/j.ijrmhm.2004.01.007.
[30] M. Yahiaoui, L. Gerbaud, J.Y. Paris, J. Denape, A. Dourfaye, A study on PDC drill bits quality, Wear 298–299 (1) (2013) 32–41. Feb, https://doi.org/10.1016/j.wear.2012.12.026.
[31] R.L. Ladi, C.E. Wells, B.K. Kataria, S.W. Almond, Chemical agents for leaching polycrystalline diamond elements, Patent US0152064A1 (2012).